POLITECNICO DI TORINO
Repository ISTITUZIONALE

On the wave attenuation properties of seagrass meadows

Original
On the wave attenuation properties of seagrass meadows / Vettori, D., Pezzutto, P., Bouma, T.J., Shahmohammadi, A., Manes, C.. - In: COASTAL ENGINEERING. - ISSN 0378-3839. - 189:(2024). [10.1016/j.coastaleng.2024.104472]

Availability:
This version is available at: 11583/2986228 since: 2024-02-22T09:19:17Z

Publisher:
Elsevier B.V.

Published
DOI:10.1016/j.coastaleng.2024.104472

Terms of use:

This article is made available under terms and conditions as specified in the corresponding bibliographic description in the repository

Publisher copyright

(Article begins on next page)

26 November 2026

Coastal Engineering 189 (2024) 104472



Contents lists available at ScienceDirect

Coastal Engineering

journal homepage: www.elsevier.com/locate/coastaleng

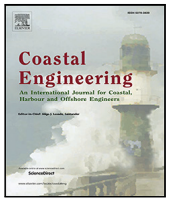

On the wave attenuation properties of seagrass meadows

Davide Vettori [a,*], Paolo Pezzutto [b], Tjeerd J. Bouma [c], Amirarsalan Shahmohammadi [a], Costantino Manes [a]

[a] Department of Environmental, Land and Infrastructure Engineering (DIATI), Politecnico di Torino, Turin, 10129, Italy
[b] National Research Council (CNR IRBIM), Ancona, 60125, Italy
[c] Royal Netherlands Institute for Sea Research, Yerseke, 4401 NT, Netherlands

ARTICLE INFO

Dataset link: https://zenodo.org/records/10512347

Keywords:
Seagrass meadow
Wave attenuation
Drag coefficient
Nature-based solution

ABSTRACT

The wave attenuation properties of seagrass meadows were investigated in a flume facility using dynamically-scaled models of seagrass exposed to regular long crested waves. Experiments were conducted for 66 wave conditions and with four plant densities; waves were measured with eight resistance wave gauges. The data collected represent the most-comprehensive dataset of its kind. They reveal that the wave attenuation coefficient K_D of a seagrass meadow reaches a uniform value after a distance of approximately 1.5–3 times the water depth from the meadow start and that both K_D and the drag coefficient C_d depend significantly on the plant density. An improved model of K_D based on the work of Lei and Nepf (2019) is proposed that takes into account the effects of the solid volume fraction of the plant model through a correction on C_d and that of plant density via an effective vegetation frontal area a_{v-e}. The effective vegetation frontal area is described as a power law of the roughness density λ_f. The model, which was validated with the data of K_D obtained from the laboratory experiments described herein, displays an excellent agreement with data from the literature. It can predict K_D accurately also for cases whereby the maximum wave orbital excursion is comparable with the blade length, despite this condition violates the model's assumptions. This work provides a comprehensive dataset and a new model that can be used to improve the prediction of wave attenuation of seagrass meadows.

1. Introduction

While traditional coastal engineering solutions are becoming economically and ecologically unsustainable (Morris et al., 2018; James et al., 2019), nature-based solutions represent an attractive alternative for coastal protection because of the range of ecosystem services they provide (Temmerman et al., 2013). In this context, seagrass canopies may have an important role in absorbing/retaining carbon, promoting biodiversity, attenuating waves and stabilizing sediments (e.g. Barbier et al., 2011; Costanza et al., 1997; Bouma et al., 2014; Greiner et al., 2013). For this reason and because of their dramatic global decline (e.g. Waycott et al., 2009), it is important that seagrass canopies are accounted for by policymakers for the development of coastal management plan (e.g. Sutton-Grier et al., 2015). However, the effectiveness of seagrass in attenuating waves, which is an important aspect of coastal protection, is still difficult to quantify as most of the literature deals with other types of nature based solutions (e.g. saltmarshes, mangroves) (e.g. Morris et al., 2018).

The first models to quantify wave attenuation due to submerged vegetation were developed by Dalrymple et al. (1984) and Kobayashi et al. (1993). Subsequent works adapted these models to laboratory datasets (e.g. Asano et al., 1988) of wave dissipation associated with kelp surrogates (e.g. Mendez and Losada, 2004; Méndez et al., 1999). A few works focused on wave attenuation due to seagrass by means of field campaigns (Fonseca and Cahalan, 1992; Bradley and Houser, 2009; Infantes et al., 2012) or laboratory experiments (e.g. Sánchez-González et al., 2011; Manca et al., 2012; Stratigaki et al., 2011). However, as argued by Twomey et al. (2020), these studies are hard to compare because they use different parameters to quantify wave attenuation (e.g. drag coefficient, wave height reduction). Twomey et al. (2020) collected all drag coefficients C_d available from the literature on seagrass and reported a mean value of $C_d = 0.7 - 1.1$ depending on the experimental conditions. In more detail, C_d was found to be a function of the Reynolds number ($Re = U_w b/\nu$, where U_w is the maximum wave orbital velocity at the vegetation top, b is the reference width of the plant and ν is the kinematic viscosity of water) (e.g. Maza et al., 2013; Bradley and Houser, 2009) and the Keulegan–Carpenter number ($KC = U_w T/b$, where T is the wave period) (e.g. Sánchez-González et al., 2011; Bradley and Houser, 2009).

More recently, Henderson (2019) developed a theoretical model for wave attenuation, which stems from scaling considerations and focuses

* Corresponding author.
E-mail address: davide.vettori@polito.it (D. Vettori).

https://doi.org/10.1016/j.coastaleng.2024.104472
Received 30 June 2023; Received in revised form 22 January 2024; Accepted 23 January 2024
Available online 24 January 2024
0378-3839/© 2024 The Authors. Published by Elsevier B.V. This is an open access article under the CC BY-NC-ND license (http://creativecommons.org/licenses/by-nc-nd/4.0/).

on the cases of small tilt, namely when the wave orbital excursion at the vegetation top is much smaller than the length of the flexible part of the plant (i.e. the blades). For the opposite case, when blade length is negligible compared to wave orbital excursion, Henderson (2019) claim that the deformation can be modelled as per unidirectional steady flows (see Luhar and Nepf, 2016). To the best of the authors' knowledge, no model has been developed for the cases wherein wave orbital excursion is comparable with blade length.

Another model was recently developed by Lei and Nepf (2019) (henceforth referred to as LN19) whereby wave attenuation is modelled by combining linear wave theory (i.e. following the approach proposed by Dalrymple et al., 1984) with a parametrization of drag based on the so-called effective length (l_e), which represents the length of a rigid vertical body that exerts the same resistance to the flow as the flexible body being studied (Luhar and Nepf, 2011). LN19 includes the reduction in orbital velocity within the canopy by means of a factor α as proposed by Lowe et al. (2005) but does not account for the plant motion in the calculation of the fluid relative velocity. It was found to agree with both laboratory data and some field data once the biomechanical properties of the vegetation in play were known (Lei and Nepf, 2019). Given these promising results, LN19 is herein used as a benchmark for the interpretation of the reported experimental results (the model is described more in depth in Section 2).

Despite these recent advances, several issues remain that limit assessing the contribution of seagrass meadows to wave attenuation. First, available models have been validated with rather limited datasets, wherein the investigated waves pertained to a small set of hydrodynamic conditions. Second, data are particularly scarce for cases in which wave orbital excursion is comparable or larger than blade length. Third, the effect of vegetation density on wave attenuation, which reflects the interactions between plants, has never been explored even though it can be significant in similar settings (see Etminan et al., 2019, for effect of vegetation density in emergent rigid canopies).

In the present work we attempt to address these issues by presenting results from laboratory experiments involving dynamically-scaled seagrass models whose wave attenuation properties were investigated for a wide range of hydrodynamic and plant density conditions. This approach is advantageous compared to field experiments because it allows to isolate the effects of various parameters without dealing with complications that are typically encountered in the field, such as poor control on plant density and health conditions (Vettori et al., 2021). We conducted experiments with four plant densities and, for each density, we tested 66 regular wave conditions varying water depth, wave period and height.

The aim of this paper is hence threefold: (i) to assess the effect of plant density on wave attenuation; (ii) to evaluate the performance of the models proposed in the literature at a wide range of conditions; and (iii) to propose a new parametrization of wave attenuation that accounts for the plant density in the meadow.

2. Theoretical background

The deflection of a flexible blade in an oscillatory flow is governed by three nondimensional parameters, the wave Cauchy number Ca_w, the buoyancy parameter B, and the blade length ratio L (Lei and Nepf, 2019):

$$Ca_w = \frac{\rho b {U_w}^2 l^3}{EI}, \tag{1}$$

$$B = \frac{(\rho - \rho_b) g b t l^3}{EI}, \tag{2}$$

$$L = \frac{l}{A_w}, \tag{3}$$

where ρ is the water density, l, b, t, $I = bt^3/12$, E, and ρ_b are the length, width, thickness, second moment of inertia (assuming a rectangular cross-section), Young's modulus, and mass density of the blade, respectively, A_w is the maximum wave orbital excursion at the canopy top (i.e. $A_w = U_w T/(2\pi)$), and g is the gravitational acceleration. The wave Cauchy number compares the hydrodynamic drag to the restoring force associated with flexural rigidity, the buoyancy parameter is the ratio of the restoring force due to buoyancy to that due to flexural rigidity, and the length ratio compares the length of the plant with the local wave excursion. For seagrass, $\rho_b \to \rho$ so that the effect of buoyancy is negligible and the blade dynamics can be described by Ca_w and L (see Luhar and Nepf, 2016).

By fitting the data of drag force for isolated seagrass models, Lei and Nepf (2019) obtained the following formula to calculate the effective length (l_e):

$$l_e/l = (0.94 \pm 0.06)(Ca_w L)^{-0.25 \pm 0.02}, \tag{4}$$

in accordance with the form originally proposed by Luhar and Nepf (2016). Eq. (4) is based on the following assumptions: (i) maximum wave excursion is much smaller than blade length (i.e. $L \gg 1$); (ii) pressure drag dominates over skin friction; (iii) $Ca_w \gg 1$ so that drag force dominates over the blade bending resistance force; and (iv) $KC \gg 1$ so that the inertial terms are negligible compared to the drag force term (the model was validated for $KC \geq 3.7$).

Wave attenuation by a submerged canopy can be explored using the conservation of energy equation and linear wave theory (Dalrymple et al., 1984), i.e.:

$$-\epsilon_D = \frac{\partial E c_g}{\partial x} = \frac{\partial}{\partial x}\left(\frac{1}{2}\rho g {a_w}^2 c_g\right), \tag{5}$$

where ϵ_D is the rate of energy dissipation, E is the wave energy (per unit wave front width), c_g is the wave group celerity, and a_w is the wave amplitude. Assuming that the vertical forces acting on the body are negligible compared to the horizontal forces (recall that $B \to 0$ for seagrass), ϵ_D can also be expressed as (Lei and Nepf, 2019):

$$-\epsilon_D = \frac{1}{T}\int_{t=0}^{T}\int_{z=0}^{l}\frac{1}{2}\rho C_d a_v |u_r| u_r u \, dz dt, \tag{6}$$

where a_v is the vegetation frontal area per unit meadow volume and u_r is the relative velocity between the vegetation and the water. Based on assumption (i) by Luhar and Nepf (2016), for most of the wave period $u_r \approx u$, where u is the absolute fluid velocity. Substituting Eq. (6) into Eq. (5) and re-arranging the terms, wave attenuation at a distance x from the start of the canopy and along the wave propagation direction can be expressed as:

$$\frac{a_w(x)}{a_w(0)} = \frac{1}{1 + K_D a_w(0) x}, \tag{7}$$

where $a_w(0)$ is the undisturbed wave amplitude, $a_w(x)$ is the wave amplitude at x, and K_D is the wave attenuation coefficient of the canopy defined as:

$$K_D = \frac{2}{9\pi} C_d a_v k \alpha^3 \left[\frac{9 sinh(k l_{eff}) + sinh(3 k l_{eff})}{sinh(kh)(sinh(2kh) + 2kh)}\right], \tag{8}$$

where k is the wavenumber, linked to the wave period T by the dispersion relation $\sigma^2 = gk \tanh kh$ (with $\sigma = 2\pi f = 2\pi/T$ being the circular frequency), and α is the ratio of in-canopy velocity to above-canopy velocity as defined by Lowe et al. (2005). Further, Lei and Nepf (2019) used a corrected effective length to account for the rigid part of the seagrass model (i.e. $l_{eff} = l_e + l_r$, with l_r defined as the rigid length), which replicates the seagrass sheath.

3. Materials and methods

3.1. Experimental design

Seagrass models were designed based on the morphological and biomechanical data available in the literature for the most common species of seagrass in Europe (namely, *Cymodocea nodosa*, *Posidonia*

Table 1
Ranges of physical parameters relevant to wave attenuation for modelled seagrass species and seagrass models employed herein and by Lei and Nepf (2019). Columns indicate: the ratio of sheath/stem length to plant length l_r/l; the number of blades per plant n_b; the plant length l; the blade width b, thickness t, Young's modulus E and mass density ρ_b; the water depth h; and the plant density n_p.

	l_r/l (%)	n_b (–)	l (m)	b (mm)	t (mm)	E (MPa)	ρ_b (g/cm^3)	h (m)	n_p (1/m^2)
C. nodosa[a]	n.a.	4	0.1–0.5	2.5–6	0.1–0.4	80	n.a.	0–5	900–1900
P. oceanica[b]	10–13	7	0.15–0.6	9–10	0.2–0.34	170–470	0.91	0.5–40	150–1200
Z. marina[c]	28–32	4	0.2–0.8	3–12	0.15–0.23	124–270	0.7–0.9	2–12	250–1500
Z. noltii[d]	n.a.	4	0.05–0.2	0.5–1.5	0.15–0.21	128–1000	n.a.	0–5	600–4600
Present study	10	4	0.1	2	0.09	128	0.92	0.15–0.6	251–1338
LN19	7	6	0.14	3	0.1	300	0.925	0.18–0.45	280–1370

[a] Cancemi et al. (2002); Olivé et al. (2013); de los Santos et al. (2013).
[b] Pergent et al. (1994); Folkard (2005); Larkum et al. (2006); De los Santos et al. (2016).
[c] Larkum et al. (2006); Fonseca et al. (2007); Ondiviela et al. (2014); Vettori and Marjoribanks (2021).
[d] Curiel et al. (1996); Paul and Amos (2011); De los Santos et al. (2016); Soissons et al. (2018).

Table 2
Summary of the wave conditions (wave frequency f and amplitude a_w) for the experiments sorted by water depth h. Note that a_w refers to the wave amplitude measured before the start of the meadow during experiments with unvegetated bed.

h (m)	0.15		0.2		0.3		0.4		0.5		0.6	
Test ID	f (Hz)	a_w (mm)	f (Hz)	a_w (mm)	f (Hz)	a_w (mm)	f (Hz)	a_w (mm)	f (Hz)	a_w (mm)	f (Hz)	a_w (mm)
1	0.46	12.5	0.72	4.0	0.61	5.0	0.88	4.5	0.9	4.0	0.67	4.5
2	0.54	15.0	0.45	14.0	0.47	8.5	0.52	9.0	0.51	7.5	1.25	9.0
3	1.07	12.5	0.52	18.5	1.22	12.0	0.47	12.5	1.25	12.5	0.59	14.5
4	0.65	18.5	0.61	20.0	0.54	23.0	1.24	20.5	1.09	23.0	0.54	21.5
5	0.86	19.5	1.15	20.5	0.7	28.0	0.6	28.0	0.56	27.0	1.16	27.0
6	0.76	22.0	1.04	25.0	1.04	34.5	1.15	33.5	1.16	34.5	1.09	36.0
7	0.96	24.0	0.84	31.0	1.12	40.0	0.67	46.5	1	44.5	1.01	45.5
8	–	–	0.95	38.5	0.82	47.0	1.07	49.5	0.64	56.0	0.73	57.5
9	–	–	–	–	0.94	56.5	0.76	59.0	0.71	71.0	0.82	69.5
10	–	–	–	–	0.7	4.5	0.99	58.5	0.8	80.0	0.92	79.0
11	–	–	–	–	0.7	14.0	0.88	13.5	1.16	4.5	–	–
12	–	–	–	–	0.7	36.0	0.88	26.0	1.16	13.0	–	–
13	–	–	–	–	0.7	52.0	0.88	34.5	1.16	26.5	–	–
14	–	–	–	–	–	–	0.88	51.0	1.16	49.5	–	–

oceanica, *Zostera marina*, *Zostera noltii*, see Table 1) and using the Froude and Cauchy similarities. Each model comprises of a rigid dowel 20 mm long to which 4 LDPE strips, which replicate the blades, are attached (see Table 1 for relevant dimensions and mechanical properties). The bottom 20 mm of the strips overlaps with the dowel so that the total length of the models is 110 mm and the external diameter of the rigid part is 3.2 mm. During the experiments, the bottom 10 mm of the rigid sheath is inserted into the false bed so that the part exposed to the waves is 100 mm long (of which the bottom 10 mm is rigid and the top 90 mm is flexible).

The seagrass models and the wave conditions were designed to replicate a very wide range of natural scenarios so that, depending on the scaling ratios being used, our experiments are representative of different species subject to a wide range of wave conditions. In more detail, six water depths were employed (from 0.15 m to 0.6 m) and for each of them 7–14 wave conditions were tested varying wave period and amplitude (see Table 2). All monochromatic waves were tested with four seagrass densities (251 plants/m^2, 502 plants/m^2, 669 plants/m^2 and 1338 plants/m^2) representative of the selected species (see Table 1) and with a smooth (unvegetated) bed.

In Fig. 1 the wave conditions used in the experiments (and listed in Table 2) are classified using Le Mehaute's plot of validity of wave theories (Le Méhauté, 2013). Most experimental conditions depart from liner wave theory, on which Eq. (6) is based. It is worth noting, however, that also Lei and Nepf (2019) performed experiments whose conditions departed from linear wave theory (see Fig. 1). In Table 3 the values of the relevant adimensional parameters governing the flow-seagrass interactions are reported for all wave conditions.

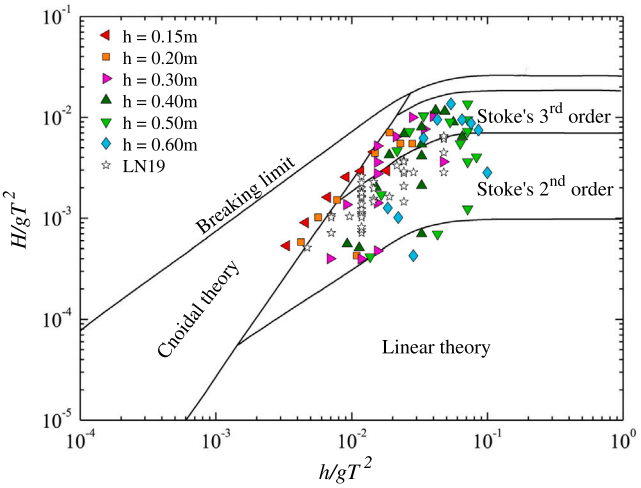

Fig. 1. Ranges of validity for wave theories as per Le Méhauté (2013). The coloured markers indicate the wave conditions used in the present work (classified by water depth), the empty stars indicate the wave conditions used by Lei and Nepf (2019).

3.2. Experimental setup and procedure

Experiments were performed in a 50 m long, 0.61 m wide and 1 m high flume facility equipped with a wavemaker at one end and a passive wave absorber at the opposite end (see Fig. 2b). Between 19 m and 23 m from the wavemaker we mounted four plexiglass baseboards pre-drilled with 2000 holes/m^2 distributed according to a staggered configuration (see Fig. 2c). In this regard, it is worth noting that the drag force of a seagrass plant within a meadow is not significantly affected by the meadow spatial arrangement (Fonseca et al., 2007), therefore we do not expect the chosen spatial arrangement to influence the wave attenuation. The baseboards were installed flush with the

Table 3
Values of the relevant dimensionless numbers (wave Cauchy number Ca_w, Keulegan–Carpenter number KC, and length ratio L) for all wave conditions sorted by water depth h.

h (m)	0.15			0.2			0.3			0.4			0.5			0.6		
Test ID	Ca_w	KC	L	Ca_w	KC	L	Ca_w	KC	L	Ca_w	KC	L	Ca_w	KC	L	Ca_w	KC	L
1	906	107	2.7	62	18	17	64	21	14	17	7.7	37	7.8	5.1	55	14	9.0	31
2	1349	111	2.6	838	105	2.8	197	49	5.9	147	38	7.9	77	28	10	1.4	1.5	181
3	838	44	6.1	1407	118	2.4	111	14	20	277	58	4.9	9.9	4.1	70	171	36	8.2
4	2029	113	2.5	1622	108	2.7	1307	109	2.6	93	13	22	90	14	20	419	62	4.6
5	2157	88	3.3	1136	48	5.8	1646	95	3.0	1201	94	3.1	853	85	3.4	29	7.6	38
6	2695	112	2.3	1905	69	4.1	1474	60	4.6	375	27	10	136	16	17	90	14	20
7	3147	95	2.8	3415	114	2.4	1637	59	4.7	3015	134	2.2	559	39	7.2	256	26	11
8	–	–	–	4820	119	2.3	4013	126	2.2	1162	52	5.4	3131	143	2.0	1752	94	3.1
9	–	–	–	–	–	–	4728	119	2.4	4069	137	2.1	4240	150	1.9	1762	84	3.4
10	–	–	–	–	–	–	48	16	18	2162	77	3.6	4165	132	2.1	1353	65	4.5
11	–	–	–	–	–	–	431	48	5.8	155	23	12	2.3	2.1	131	–	–	–
12	–	–	–	–	–	–	2785	123	2.2	601	45	6.3	20	6.3	45	–	–	–
13	–	–	–	–	–	–	5718	176	1.6	1045	60	4.7	80	13	22	–	–	–
14	–	–	–	–	–	–	–	–	–	2271	88	3.2	277	23	12	–	–	–

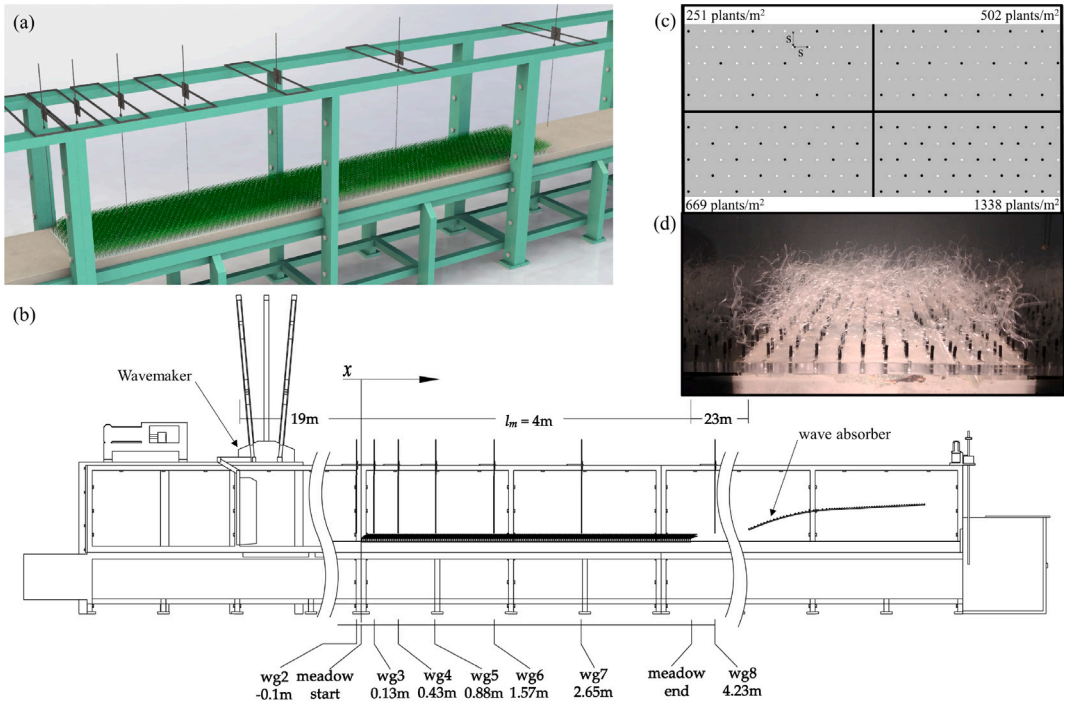

Fig. 2. Overview of the experimental setup: (a) rendering of the part of the flume covered by the seagrass meadow; (b) lateral view of the flume facility with longitudinal coordinates of the meadow and of the wave gauges (i.e. wgs) and distance from the meadow to the wavemaker and the wave absorber; (c) spatial arrangement of staggered holes and plants (filled circles) for the four seagrass densities used; (d) photo of seagrass meadow with 1338 plant/m^2 during experiments.

flume bed and fixed in place by means of anchoring structures and silicone. A 0.1 mm thick adhesive film was applied on the upper surface of the baseboards to exclude any effect of the holes on wave attenuation. For experiments with a vegetated bed, seagrass models were inserted into the baseboards according to the staggered configurations reported in Fig. 2c.

Water surface displacement was measured using a set of eight resistance wave gauges controlled with a PC via a dedicated software (Edinburgh Designs, Edinburgh, UK). The analogue signal from the gauges is converted into a digital signal by a controller that also ensures that gauges measure synchronously. Gauges were located along the channel (see Fig. 2a-b) so that one gauge recorded the wave generated – 2 m from the wavemaker paddle – and the remaining gauges were located along the seagrass meadow as follows: one gauge 0.1 m from the start of the meadow, five gauges at incremental distances along the meadow and one gauge 0.23 m after the meadow's end (see Fig. 2b). During experiments, wave gauges were triggered by the wavemaker and data were sampled at 128 Hz for over 100 wave cycles.

3.3. Data analysis

The model described in Section 2 rests on the hypothesis of linear long-crested waves. Most of the experimental conditions depart from Airy wave conditions, thus weakly nonlinear effects in the flume are to be expected, especially for sinusoidal motion of the wavemaker (see e.g. Schaffer, 1996). We neglect potential contamination by relevant modulations of the carrier because these phenomenon develops at length scales which are much larger than the flume length. On the other hand, the amplitudes of second and higher harmonics vary at shorter scales, and their presence is not contemplated by the model described in Section 2. With this in mind, the timeseries of the water surface displacement η acquired with the wave gauges were pre-processed with a bandpass filter to remove higher order harmonics and very long waves. The bandpass filter was centred on the generation frequency f used by the wavemaker and had a width of 25% f on either side.

The filtered signal from the last wave gauge (i.e. wave gauge 8) was trimmed to exclude the initial wavemaker transients and avoid

contamination due to reflection from the passive absorber. Such trimming was defined on the basis of the group celerity and allowed to isolate a wave train whose duration covers the largest possible number of integer periods depending on the wave characteristics. The wave train thus identified for wave gauge 8 was then isolated in the signals from wave gauges 2–7, with the initial time shifted according to the group celerity, so that the same waves along the meadow would be analysed and compared. The mean wave amplitude a_{w_i} at wave gauge i was estimated from the root mean square of η_i as:

$$a_{w_i} = \sqrt{\frac{2}{t_{end}} \int_{t=0}^{t_{end}} \eta_i^2(t) dt}, \tag{9}$$

where t_{end} is the time length of the isolated wave train, and $\eta_i(t)$ is the filtered water surface displacement at wave gauge i at the time t.

For each test, the wave attenuation coefficient K_D due to the seagrass meadow was estimated from the observations at wave gauges 2–8 as follows:

(i) Eq. (7) was re-arranged as:

$$y(x) = K_D x,$$
$$\text{with } y(x) = \frac{a_w(0) - a_w(x)}{a_w(x) a_w(0)}. \tag{10}$$

(ii) the wave attenuation coefficient K_{D0} for the unvegetated bed was calculated by least-square fitting $y(x)$ to the data collected at wave gauges 2 to 8;

(iii) the total wave attenuation coefficient K_{D-tot} for a vegetated bed was calculated by least-square fitting $y(x)$ to the data collected at gauges 2 to 8 for 0 m $< x <$ 4 m, i.e. where the meadow is located;

(iv) the wave attenuation coefficient due to the seagrass meadow K_D was calculated as $K_D = K_{D-tot} - K_{D0}$, thus assuming linear superposition between the wave attenuation associated with the facility and that of the meadow.

For modelling the wave attenuation coefficient (see Section 2), the maximum wave orbital velocity U_w at the top of the meadow was estimated as per linear wave theory, i.e.:

$$U_w = 2\pi f a_{w_2} \frac{\cosh kl}{\sinh kh}, \tag{11}$$

where a_{w_2} is the wave amplitude at wave gauge 2.

3.4. Experiments with unvegetated bed

All wave conditions listed in Table 2 were tested with an unvegetated bed to obtain an estimate of the wave attenuation coefficient due to the smooth bed and lateral walls of the flume. The values of K_{D0} obtained from measurements were compared with estimates from Hunt's theory (Hunt, 1952), which is valid for a smooth channel and is based on linear wave theory, i.e.:

$$K_{d0} = \frac{2k}{B} \sqrt{\frac{\nu}{2\sigma}} \frac{kB + sinh(2kh)}{2kh + sinh(2kh)}, \tag{12}$$

where ν is the water kinematic viscosity and B is the channel width. It is worth noting that Hunt (1952) modelled wave attenuation as a negative exponential function (i.e. $a_w(x)/a_w(0) = \exp(-K_{d0}x)$). This form is equivalent to the hyperbolic form derived by Dalrymple et al. (1984, see Eq. (7)) as long as $K_{d0}x < 0.1$, which is true for all experiments with unvegetated bed considered herein. To compare the two coefficients, we converted K_{D0} into $K_{d0} = K_{D0}a_w(0)$. The results of the analysis are reported in Fig. 3, where K_{d0} calculated from measurements are plotted together with the estimates from Hunt's theory. For most conditions, measured K_{d0} are comparable with the theoretical values, but for $kh <$ 0.5 a few points deviate by almost an order of magnitude from Hunt's theory. These deviations, however, do not influence significantly the results of the present work because in shallow waters the attenuation due to the seagrass meadow is much larger than that due to the facility.

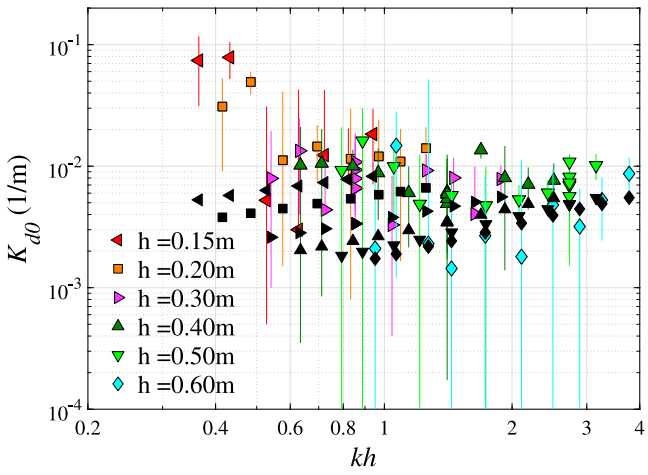

Fig. 3. Wave attenuation coefficient K_{d0} of the unvegetated bed as a function of kh. The coloured markers indicate the measured K_{d0} (the 95% confidence intervals from linear regression are included as vertical bars) and the black markers indicate the respective K_{d0} estimated as per Hunt's theory (Hunt, 1952). Note that markers are sorted by water depth.

4. Results

4.1. Wave attenuation along the meadow

As first step in our analysis, we assess how waves are attenuated along the meadow, as this provides information about the uncertainty associated with the estimation of K_D and reveals potential spatial inhomogeneities that should be taken into account in future studies. To do so, we use Eq. (10) to estimate K_{D-tot} locally between each pair of adjacent a_{w_i} from the start to the end of the meadow (see Fig. 2b). In practice, we calculate $K_{D-tot}(x_j)$ as:

$$K_{D-tot}(x_j) = \frac{a_{w_{i-1}} - a_{w_i}}{a_{w_{i-1}} a_{w_i} \left(x_i - x_{i-1}\right)}, \tag{13}$$

with $x_j = (x_i + x_{i-1})/2$.

The local estimate $K_{D-tot}(x_j)$ varies significantly along the meadow and shows a strong deviation from the 'global' estimate K_{D-tot} ('global' in the sense that it is obtained from linear regression for 0 m$< x <$ 4 m, as described in Section 3.3).

In most cases, the local attenuation coefficient differs significantly from K_{D-tot} for $x < 1.5 - 3h$ (see some examples in Fig. 4, wherein $\delta_K(x_j) = (K_{D-tot}(x_j) - K_{D-tot})/K_{D-tot}$). The reason for this is not clear, but we hypothesize that it is due to the discontinuity between the unvegetated bed and the meadow. As an abrupt change, such discontinuity may involve the generation of local evanescent modes (see e.g. Massel, 1983), which can lead to local deviations from the linear progressive wave condition, hence compromising the assumptions on which Eq. (5) is based. To support our experimental findings, we note that the amplitude of the largest disturbance of this kind decays following $\exp(-k_1 x)$, with x being the distance from the discontinuity and k_1 being the smallest root of $\sigma^2 + gk_n \tan k_n h = 0$, and attains 1% of its maximum value at about $1.5h$ in shallow waters, and about $3h$ in deep waters. Therefore, we suggest that measurements should be taken sufficiently far away from the bottom transition for an accurate quantification of the wave attenuation seagrass meadows.

Infantes et al. (2012) reported that the friction factor increased with distance over 1000 m in a natural meadow, hence supporting that wave attenuation coefficient is not constant in x. However, in the present study the length of the meadow is much smaller than what can be found in the field, hence impeding any critical comparison between our results and those of Infantes et al. (2012).

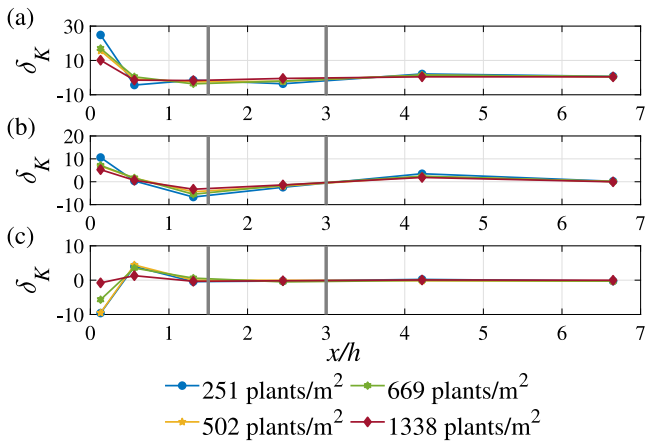

Fig. 4. Relative error δ_K in the local wave attenuation coefficient along the meadow compared to the 'global' estimate of K_{D-tot}, which is used as reference value. The relative error is reported for three experiments conducted with $h = 0.5$ m for all plant densities: (a) corresponds to Test ID1 (see Table 2), (b) corresponds to Test ID2, and (c) corresponds to Test ID3. The vertical grey lines indicate $x = 1.5h$ and $x = 3h$.

4.2. Wave attenuation models

The comparison of our results with existing models of wave attenuation by seagrass meadows is organized into two parts. In the first part, we consider models of the drag coefficient of seagrass meadows proposed in the literature – note that such drag coefficient is then used to model the wave attenuation coefficient as per Dalrymple et al. (1984) or Kobayashi et al. (1993) –; in the second part, we employ the model of K_D developed by Lei and Nepf (2019) that makes use of the concept of effective length.

4.2.1. Models based on C_d

We calculate the drag coefficient C_d of seagrass models from the measured wave attenuation coefficient K_D considering the undeflected length of the plants (as per original formulation by Dalrymple et al., 1984) and assuming that the in-canopy flow velocity is equal to the above-canopy flow velocity so that our estimates of C_d are comparable to the relevant literature, i.e.:

$$C_d = \frac{9\pi}{2} K_D \frac{sinh(kh)(sinh(2kh) + 2kh)}{a_v k(9sinh(kl) + sinh(3kl))}. \quad (14)$$

It is worth noting that such an estimate of C_d is double-averaged (in time throughout several waves and in space along and across the meadow). The values of C_d thus obtained are displayed versus the Keulegan–Carpenter (KC) and Reynolds (Re) numbers in Fig. 5. All cases with $C_d < 0$, which is clearly unphysical, are characterized by $KC < 7$ (see Fig. 5), suggesting that in the inertia-dominated regime the meadow length is not sufficient to estimate wave attenuation accurately or the theoretical framework underpinning the definition of C_d as in Eq. (14) breaks down completely.

Data show a clear stratification depending on the plant density that likely occurs due to the sheltering phenomenon between adjacent plants that become stronger as plant density increases (see Fig. 5c-d). In the best fit models of the form $C_d \sim KC^{-\gamma}$ and $C_d \sim Re^{-\delta}$ (note that $\sim$ means "scales as"), the exponents γ and δ vary within 0.73–0.87 and 0.75–0.87, respectively, with no significant dependence on plant density. We then impose two conditions: (i) $KC \geq 7$; and (ii) $ka \leq 0.1$ and $kh \leq 2$. Condition (i) is akin to imposing $KC \gg 1$ as per Dalrymple et al. (1984) and excludes cases in which inertial forces are likely to be equal or larger than drag forces (see empty markers in Fig. 5). Condition (ii) excludes cases wherein waves are very steep and simultaneously deep water conditions are approached (see filled black markers in Fig. 5). The exact reasons why these cases deviate so much from the others is not clear. In deep waters (high kh), the interaction with the bottom is limited due to the negligible orbital motion. If the steepness (ka) is sufficiently high, the strong spatial gradients may induce localized dissipation. Clearly, these phenomena have to be modelled considering high order nonlinear corrections and including different proper dissipation terms, departing from the theoretical framework of Eq. (14). Nevertheless, for the cases described, our hypothesis is that the energy losses at the surface, due to the high steepness ($ka > 0.1$) are probably higher than the energy losses due to the (negligible) interaction at the bottom. Re-calculating the best fits after removing cases that violate conditions (i) or (ii), we obtain $\gamma = 0.64 - 0.77$ and $\delta = 0.62 - 0.71$.

Further, we compare our models with the C_d-based models from the relevant literature. We exclude the models validated with data from kelp physical surrogates (e.g. Kobayashi et al., 1993; Mendez and Losada, 2004) and focus on those validated with data from seagrass meadows (either natural or modelled). The empirical relationships obtained by Bradley and Houser (2009) do not fit our data (see Fig. 5c-d) despite the seagrass meadows investigated therein had a density of 1100 plant/m^2, thus compatible with our experiments. The reason for this difference is not clear and cannot be further explored with the data available. The empirical relationships reported by Sánchez-González et al. (2011) and Maza et al. (2013) follow the trend of our data slightly better, particularly $C_d = 0.87 + (2200/Re)^{0.88}$ (Maza et al., 2013), whose exponent agrees with those calculated from our data, but are not good fits. The likely reason for such divergences are the different properties of the seagrass meadows employed: Maza et al. (2013) validated their model with the experimental data from Stratigaki et al. (2011), whose seagrass models were stiffer and more buoyant than the models used in the present work, hence exerted a higher resistance to the flow; Sánchez-González et al. (2011) validated their model for a seagrass meadow with 40,000 plant/m^2, which may generated a strong sheltering effect thus reducing C_d.

4.2.2. Model by Lei and Nepf (2019)

Next, we compare the wave attenuation coefficients K_D calculated from our experimental data with the predictions of LN19 based on the concept of effective length (Lei and Nepf, 2019). We recall that the rigid length l_r of the seagrass model is included in the calculation of the effective length $l_{eff} = l_e + l_r$, with l_e defined in Eq. (4). In their work, Lei and Nepf (2019) tuned the length of the rigid part according to video-monitored blade deflection, obtaining $l_r = 1.6$ cm. Instead, we stick to the fact that the rigid part of our blades is fixed by construction, $l_r = 1$ cm, corresponding to the exposed length of the dowel in our seagrass models (see Table 1). We calculate the ratio of in-canopy flow velocity to above-canopy flow velocity α as per Lowe et al. (2005) and use $C_d = max(10KC^{-1/3}, 1.95)$ for the blades (Luhar and Nepf, 2016) and $C_d = 1.8$ for the rigid stem (Keulegan and Carpenter, 1958). The results are displayed in Fig. 6a: the model strongly underpredicts our experimental data and the predicted K_D have a 0.36:1 agreement with the measured K_D ($R^2 = 0.90$).

The model's deviation from our data suggests that l_{eff} is underestimated and the most obvious reason for this is that EI of the LDPE strips is not representative of the effective flexural rigidity of the seagrass models. This may happen because of twisting and bending of the strips, and of the way in which the strips were attached to the dowel. To quantify these effects, we conducted cantilever bending tests on 30 seagrass models: the dowel was clamped on an horizontal plane and the blades were free to bend in air under their own weight. The maximum deflection thus recorded was compared with the predictions from nonlinear theory in the same conditions. We found the second moment of inertia of the seagrass models to be on average 8 times larger than the theoretical value for a rectangular cross-section. Therefore, we correct our model using $I = 2bt^3/3$, which improves the model performance to a 0.48:1 agreement ($R^2 = 0.90$). Stemming from this result, to prevent

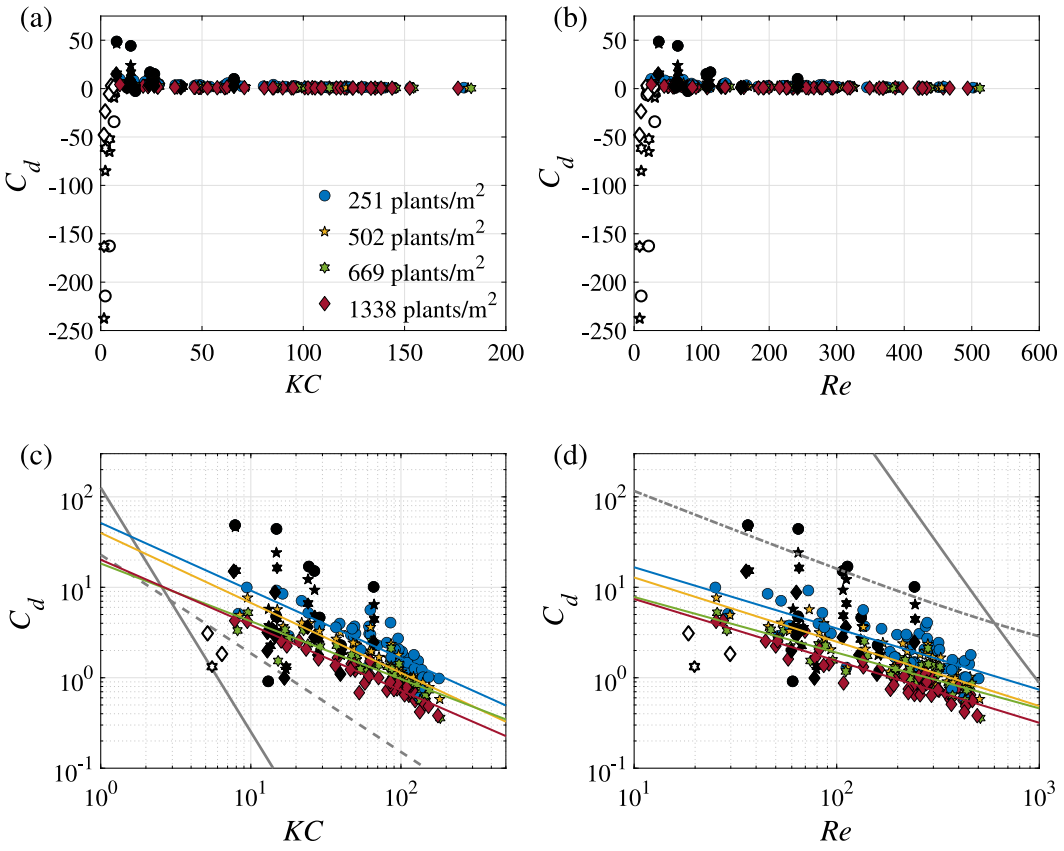

Fig. 5. Drag coefficient as a function of the Keulegan–Carpenter (a-c) and Reynolds (b-d) numbers. The empty markers indicate cases wherein $KC < 7$, the filled black markers indicate cases wherein $ka > 0.1$ and $kh > 2$. In (c-d) the best linear fits for each plant density are plotted with solid lines, the solid grey lines denote the models reported by Bradley and Houser (2009) (i.e. $C_d = 126.45KC^{-2.7}$ and $C_d = 0.1 + (925/Re)^{3.16}$), the dashed grey line in (c) denotes the model reported by Sánchez-González et al. (2011) (i.e. $C_d = 22.9KC^{-1.09}$) and the dash-dotted grey line in (d) denotes the model reported by Maza et al. (2013) (i.e. $C_d = 0.87 + (2200/Re)^{0.88}$).

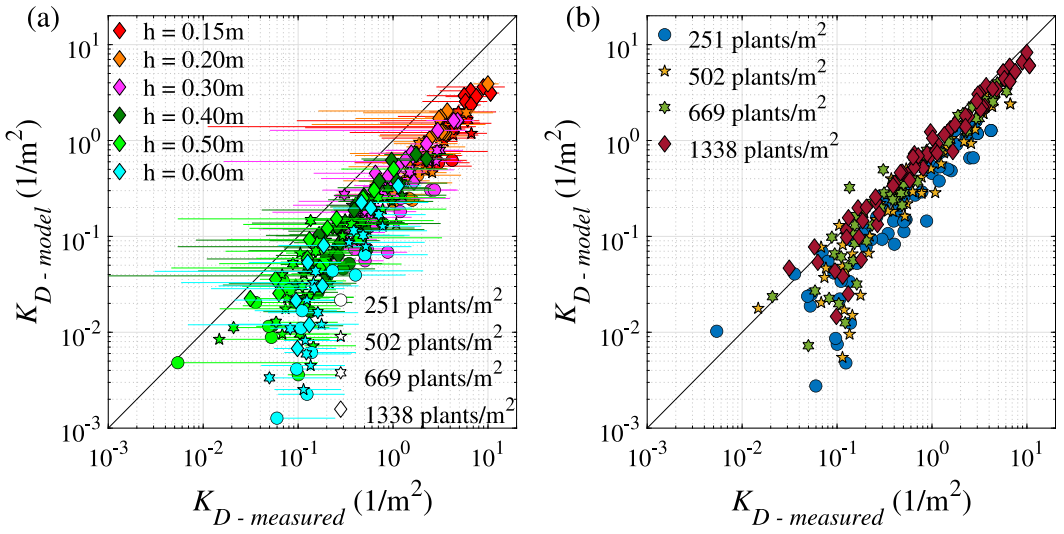

Fig. 6. Measured K_D versus K_D predicted from Eq. (8): as per Lei and Nepf (2019) (a) and after corrections to I and C_d (b). The solid lines denote a 1:1 agreement. In (a) 95% confidence interval (CI) in both measured and predicted K_D is included: CI in measured K_D is quite large because of the limited number of wave gauges employed. To ease data visualization, CI is not included in (b).

potential biases, we recommend that in similar studies flexural rigidity is measured on the plant models rather than on the blades.

To explain this remaining underestimation we consider the effect of seagrass model geometry on C_d. Based on recent findings on the drag force of a patch of rigid cylinders immersed in a turbulent boundary layer (e.g. Taddei et al., 2016), we expect C_d of a bundle of blades to exceed that of an individual blade. In particular, Taddei et al. (2016) reported that C_d varies with the solid volume fraction of the bundle/patch, which is equal to 0.09 for the seagrass models employed herein (the solid volume fraction was calculated assuming the blades to be undeflected), leading to an increase in C_d of 54% compared to that of a filled volume according to their results. With this second correction

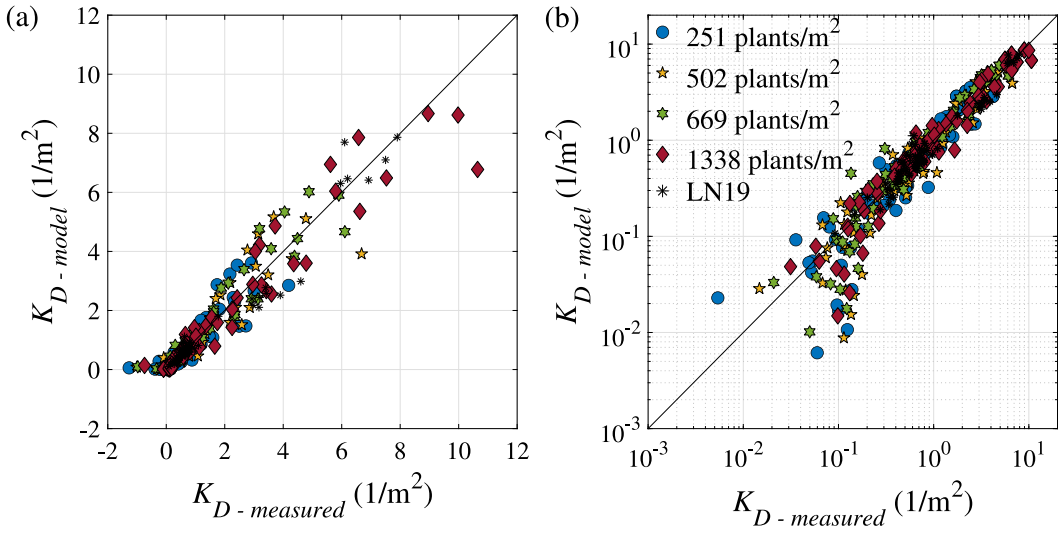

Fig. 7. Measured wave attenuation coefficient versus K_D predicted from Eq. (17): in linear scales (a) and log scales (b). The solid line denotes a 1:1 agreement.

the agreement between K_D predicted by the model and the measured K_D further improves to 0.69:1 ($R^2 = 0.91$, see Fig. 6b).

For the seagrass models employed by Lei and Nepf (2019), the solid volume fraction is equal to 0.05, leading to an increase in C_d of 17% according to the results of Taddei et al. (2016). Applying this correction to the data from Lei and Nepf (2019), and setting $l_r = 1$ cm, which corresponds to the dowel length used therein (rather than $l_r = 1.6$ cm), improves the model agreement from 1:1.28 ($R^2 = 0.95$) to 1:1.14 ($R^2 = 0.94$) – note that the model agreement was calculated using the data made available by Lei and Nepf (2019) and recalculating α independently. Thus, accounting for the effect of the bundle of blades on C_d we remove the need to tune l_r, which corroborates the validity of our approach.

4.3. On the effect of plant density

Looking at Fig. 6b it is evident that a stratification of data depending on plant density exists for K_D (similar to what displayed for C_d in Fig. 5c-d). The stratification backs the idea that there exists a significant effect of sheltering and blockage (e.g. Etminan et al., 2019) in seagrass meadows in contrast with recent findings by Lei and Nepf (2019). In Eq. (8) the plant density indirectly affects K_D because it is incorporated in the calculation of α (Lowe et al., 2005), wherein higher densities lead to lower α, hence compensating, at least partially, for the effect of sheltering on K_D. In principle, α was designed to describe the effect of sheltering through the reduction of in-canopy flow velocity but it does not account for any blockage effect and was developed for rigid canopies, hence may not work as well for flexible canopies. Indeed, if we apply the effective length in the calculation of α, the discrepancy between the modelled and the measured K_D enlarges.

A physically-based parameter that allows to describe the effect of plant density on the flow is the ratio of canopy frontal area A_f to underlying bed surface area A_t (e.g. Chung et al., 2021; Britter and Hanna, 2003), also referred to as roughness density (Wooding et al., 1973), i.e.:

$$\lambda_f = A_f/A_t = \left[n_b b(l - l_r) + d l_r\right] n_p, \tag{15}$$

where d is the diameter of the rigid part of the seagrass model and the other quantities are defined in Table 1. It is worth noting that all values of λ_f considered herein fall within the range of dense canopies (i.e. $\lambda_f > 0.15$) according to Nepf (2012): λ_f ranged from 0.19 (for 251 plants/m^2) to 1.01 (for 1338 plant/m^2) in our experiments, while it varied from 0.54 to 2.03 in Lei and Nepf (2019). Interestingly, the trend of C_d versus plant density (see Figs. 5c-d) agrees with the findings of drag in rough surfaces (e.g. Chung et al., 2021) (seagrass meadow is herein considered as a rough surface) according to which drag decreases monotonically for $\lambda_f > 0.15 - 0.3$. To the best of our knowledge, such a trend has never been verified for submerged canopies exposed to waves.

By comparing the K_D predicted from LN19 corrected as described in Section 4.2.2 and our data sorted by plant density, we note that the model is tuned to work reasonably well for high plant densities and its agreement decreases strongly as plant density lowers: from the lowest to the highest plant density considered herein, the agreement is 0.41:1 ($R^2 = 0.82$), 0.56:1 ($R^2 = 0.85$), 0.68:1 ($R^2 = 0.94$) and 0.73:1 ($R^2 = 0.95$), respectively. This trend appears to be in line with the range of λ_f used to validate LN19 and indicates that the model underpredicts K_D at low λ_f, where we expect C_d to be larger.

Because sheltering/blockage effect reduces/increases the canopy frontal area 'felt' by the flow, we quantify it by introducing an effective vegetation frontal area a_{v-e} per unit meadow volume (recall that $a_v = \lambda_f/l$), i.e.:

$$a_{v-e} = \varepsilon \frac{\lambda_f^{1-\beta}}{l}, \tag{16}$$

where ε and β are numerical coefficients, and β varies between 0 and 1. According to this formulation, when $\lambda_f < \sqrt[\beta]{\varepsilon}$, a_{v-e} is larger than a_v, hence implying that the blockage effect is dominant and that the drag force is larger than what expected for a_v. On the other hand, when $\lambda_f > \sqrt[\beta]{\varepsilon}$, a_{v-e} is smaller than a_v meaning that the sheltering effect is more important and that the drag force is reduced compared to that expected for a_v. In this context ε acts as a scaling factor, without which the cross-over between the two regimes would be imposed at $\lambda_f = 1$.

Since K_D is a measure of the drag force exerted by the flow on the canopy, with no sheltering/blockage effect we expect that $K_D \sim \lambda_f$ and $C_d \sim \lambda_f^{-1}$ (see Eqs. (8) and (14), respectively). We estimated the values of ε and β from our experiments by fitting C_d versus λ_f for all the wave conditions listed in Table 2 excluding cases with (i) $KC < 7$, and (ii) $ka > 0.1$ and $kh > 2$, consistent with what discussed in Section 4.2.1. As mean values, we obtained $\varepsilon = 1.12$ and $\beta = 0.48$.

To account for the effect of plant density on the in-canopy flow, we propose a new model of K_D that includes the effective vegetation frontal area a_{v-e}, i.e.:

$$K_D = \frac{2}{9\pi} C_d a_{v-e} k \left(\frac{9 sinh(k l_{eff}) + sinh(3 k l_{eff})}{sinh(kh)(sinh(2kh) + 2kh)} \right), \tag{17}$$

where α is removed, a_{v-e} is calculated using $\beta = 0.48$ and $\varepsilon = 1.12$, and C_d is corrected as described in Section 4.2.2. Fig. 7 shows that the

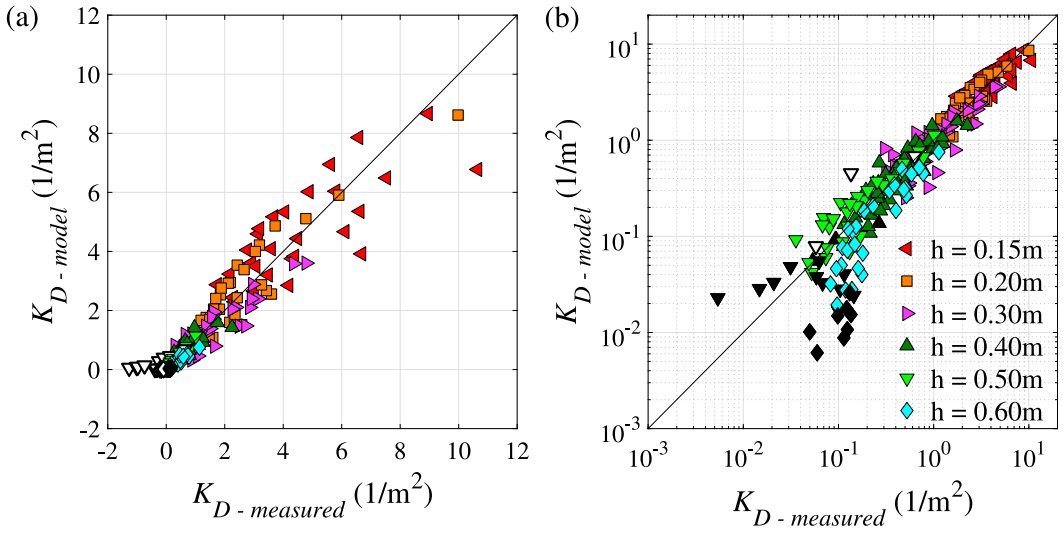

Fig. 8. Measured wave attenuation coefficient versus K_D predicted from Eq. (17) sorted by water depth: in linear scales (a) and log scales (b). Empty markers indicate cases with $KC < 7$, filled black markers cases with $kh > 2$ and $ka > 0.1$. The solid lines denote a 1:1 agreement.

predictions from Eq. (17) for our data and those of Lei and Nepf (2019) are very accurate, with an agreement between modelled and measured K_D of 1.02:1 ($R^2 = 0.90$) and 1.07:1 ($R^2 = 0.95$), respectively.

4.4. Discussion on model's performance

The predictions of the model defined in Eq. (17) fit our dataset well despite many of our tests did not meet the assumptions on which it is based, in particular: (i) $KC \gg 1$, and (ii) $L \gg 1$.

Eq. (17) (like all previous models based on Dalrymple et al., 1984) considers the wave attenuation by the seagrass meadows to be mainly caused by the drag force, while inertial forces are negligible (note that such condition is strictly met if $KC \gg 1$). In the present work KC ranges between 1.5 and 184 (see Table 3), hence including cases whereby inertial terms are expected to dominate seagrass dynamics. Similar to what displayed in Fig. 5a, when $KC < 7$, K_D calculated according to Eq. (17) attains negative values (see empty markers in Fig. 8a), indicating that violating this model's assumption impedes a correct definition of the wave attenuation coefficient. This suggests that the meadow is weakly dissipating and a longer meadow would be required to observe measurable wave attenuation coefficients K_D. Similar considerations can be deduced from the deviations between measurements and predictions for $kh > 2$ and $ka > 0.1$ (see black markers in 8b), namely as we approach deep water conditions and waves are steep.

The assumption $L \gg 1$ (see Luhar and Nepf, 2016) implies that the seagrass models experience small deflections (and hence Eq. (4) is valid). In our experiments $L = 1.6 - 181$ (see Table 3), thus we expect the deviations of the predicted K_D from our measurements to show a dependence on L when moving away from the underlying assumption of approaching small blade length ratio (i.e. $L \approx 1$). On the contrary, we do not observe such expected behaviour. This possibly implies that any corrections to account for large excursion of the blade should be negligible.

5. Conclusions

In this work we explored the wave attenuation properties of seagrass meadows via experiments with dynamically-scaled surrogates of seagrass in a flume facility. The experiments were performed with four plant densities (from 251 plant/m^2 to 1338 plant/m^2) and covering a wide range of wave conditions. Our results were compared with existing models of the drag coefficient C_d and of the wave attenuation coefficient K_D of seagrass meadows.

Our analysis indicated that waves are not attenuated uniformly along the meadow and an accurate estimate of K_D can be attained at a distance from the meadow start greater than approximately $1.5 - 3h$. Modelling K_D by exploiting the concept of effective length l_e appeared to be more promising than modelling C_d via empirical fittings, which is very sensitive to experimental conditions and needs a fine tuning of key parameters. Both the C_d and K_D obtained from our experiments showed an evident dependence on the plant density which suggests that sheltering/blockage effect is important in describing the interaction between waves and seagrass meadows.

We described and validated a new model to predict K_D based on the work of Lei and Nepf (2019). The model contains two main novelties: (i) the drag coefficient C_d of the blades was adjusted to account for the effect of the solid volume fraction of the plant model; and (ii) the effective vegetation frontal area $a_{v-e} = \varepsilon \lambda_f^{1-\beta}/l$ was introduced to quantify the effect of sheltering. In more detail, we found that $\varepsilon = 1.12$ and $\beta = 0.48$ as mean values across our tests.

Our models showed a very good agreement with the data collected for the present study (1.02:1, with $R^2 = 0.90$) and those from Lei and Nepf (2019) (1.07:1, with $R^2 = 0.95$) even for large plant deflections ($L \to 1$), thus improving significantly the model's accuracy with respect to previous works.

CRediT authorship contribution statement

Davide Vettori: Conceptualization, Data curation, Formal analysis, Funding acquisition, Investigation, Methodology, Project administration, Resources, Supervision, Validation, Writing – original draft, Writing – review & editing. **Paolo Pezzutto:** Formal analysis, Methodology, Writing – review & editing, Writing – original draft. **Tjeerd J. Bouma:** Conceptualization, Supervision. **Amirarsalan Shahmohammadi:** Investigation. **Costantino Manes:** Conceptualization, Supervision, Writing – review & editing.

Declaration of competing interest

The authors declare that they have no known competing financial interests or personal relationships that could have appeared to influence the work reported in this paper.

Data availability

Data supporting the conclusions of this publication can be found in the open access repository Zenodo at the following link: https://zenodo.org/records/10512347.

Acknowledgements

The authors wish to thank: F. Giordana for his help manufacturing seagrass models and conducting the experiments, R. Bosio and A. Cagninei for thorough technical support. The project leading to this publication has received funding from the European Union's Horizon 2020 research and innovation programme under the Marie Sklodowska-Curie grant agreement No 101022685.

References

Asano, T., Tsutsui, S., Sakai, T., 1988. Wave damping characteristics due to seaweed. In: Proc. 25th Coastal Eng. Conf. in Japan. Japan Society of Civil Engineers, Tokyo, pp. 138–142.

Barbier, E.B., Hacker, S.D., Kennedy, C., Koch, E.W., Stier, A.C., Silliman, B.R., 2011. The value of estuarine and coastal ecosystem services. Ecol. Monograph. 81 (2), 169–193.

Bouma, T.J., Van Belzen, J., Balke, T., Zhu, Z., Airoldi, L., Blight, A.J., Davies, A.J., Galvan, C., Hawkins, S.J., Hoggart, S.P., et al., 2014. Identifying knowledge gaps hampering application of intertidal habitats in coastal protection: Opportunities & steps to take. Coast. Eng. 87, 147–157.

Bradley, K., Houser, C., 2009. Relative velocity of seagrass blades: Implications for wave attenuation in low-energy environments. J. Geophys. Res.: Earth Surface 114 (F1).

Britter, R.E., Hanna, S.R., 2003. Flow and dispersion in urban areas. Annu. Rev. Fluid Mech. 35 (1), 469–496.

Cancemi, G., Buia, M.C., Mazzella, L., 2002. Structure and growth dynamics of Cymodocea nodosa meadows. Sci. Mar. 66 (4), 365–373.

Chung, D., Hutchins, N., Schultz, M.P., Flack, K.A., 2021. Predicting the drag of rough surfaces. Annu. Rev. Fluid Mech. 53, 439–471.

Costanza, R., d'Arge, R., De Groot, R., Farber, S., Grasso, M., Hannon, B., Limburg, K., Naeem, S., O'neill, R.V., Paruelo, J., et al., 1997. The value of the world's ecosystem services and natural capital. Nature 387 (6630), 253–260.

Curiel, D., Bellato, A., Rismondo, A., Marzocchi, M., 1996. Sexual reproduction of Zostera noltii Hornemann in the lagoon of Venice (Italy, north Adriatic). Aquatic Bot. 52 (4), 313–318.

Dalrymple, R.A., Kirby, J.T., Hwang, P.A., 1984. Wave diffraction due to areas of energy dissipation. J. Waterw., Port, Coastal, Ocean Eng. 110 (1), 67–79.

de los Santos, C.B., Brun, F.G., Vergara, J.J., Pérez-Lloréns, J.L., 2013. New aspect in seagrass acclimation: leaf mechanical properties vary spatially and seasonally in the temperate species Cymodocea nodosa Ucria (Ascherson). Mar. Biol. 160, 1083–1093.

De los Santos, C.B., Onoda, Y., Vergara, J.J., Pérez-Lloréns, J.L., Bouma, T.J., La Nafie, Y.A., Cambridge, M.L., Brun, F.G., 2016. A comprehensive analysis of mechanical and morphological traits in temperate and tropical seagrass species. Mar. Ecol. Prog. Ser. 551, 81–94.

Etminan, V., Lowe, R.J., Ghisalberti, M., 2019. Canopy resistance on oscillatory flows. Coast. Eng. 152, 103502.

Folkard, A.M., 2005. Hydrodynamics of model posidonia oceanica patches in shallow water. Limnol. Oceanogr. 50 (5), 1592–1600.

Fonseca, M.S., Cahalan, J.A., 1992. A preliminary evaluation of wave attenuation by four species of seagrass. Estuar. Coast. Shelf Sci. 35 (6), 565–576.

Fonseca, M.S., Koehl, M., Kopp, B.S., 2007. Biomechanical factors contributing to self-organization in seagrass landscapes. J. Exp. Mar. Biol. Ecol. 340 (2), 227–246.

Greiner, J.T., McGlathery, K.J., Gunnell, J., McKee, B.A., 2013. Seagrass restoration enhances "blue carbon" sequestration in coastal waters. PLoS One 8 (8), e72469.

Henderson, S.M., 2019. Motion of buoyant, flexible aquatic vegetation under waves: simple theoretical models and parameterization of wave dissipation. Coast. Eng. 152, 103497.

Hunt, J., 1952. Viscous damping of waves over an inclined bed in a channel of finite width. Houille Blanche 836–842.

Infantes, E., Orfila, A., Simarro, G., Terrados, J., Luhar, M., Nepf, H., 2012. Effect of a seagrass (Posidonia oceanica) meadow on wave propagation. Mar. Ecol. Prog. Ser. 456, 63–72.

James, R.K., Silva, R., Van Tussenbroek, B.I., Escudero-Castillo, M., Mariño-Tapia, I., Dijkstra, H.A., Van Westen, R.M., Pietrzak, J.D., Candy, A.S., Katsman, C.A., et al., 2019. Maintaining tropical beaches with seagrass and algae: a promising alternative to engineering solutions. BioScience 69 (2), 136–142.

Keulegan, G.H., Carpenter, L.H., 1958. Forces on cylinders and plates in an oscillating fluid. J. Res. Natl. Bur. Stand. 60 (5), 423–440.

Kobayashi, N., Raichle, A.W., Asano, T., 1993. Wave attenuation by vegetation. J. Waterw., Port, Coastal, Ocean Eng. 119 (1), 30–48.

Larkum, A.W., Orth, R.J., Duarte, C.M., 2006. Seagrasses: Biology, Ecology and Conservation. Springer.

Le Méhauté, B., 2013. An Introduction to Hydrodynamics and Water Waves. Springer Science & Business Media.

Lei, J., Nepf, H., 2019. Wave damping by flexible vegetation: Connecting individual blade dynamics to the meadow scale. Coast. Eng. 147, 138–148.

Lowe, R.J., Koseff, J.R., Monismith, S.G., Falter, J.L., 2005. Oscillatory flow through submerged canopies: 2. Canopy mass transfer. J. Geophys. Res.: Oceans 110 (C10).

Luhar, M., Nepf, H.M., 2011. Flow-induced reconfiguration of buoyant and flexible aquatic vegetation. Limnol. Oceanogr. 56 (6), 2003–2017.

Luhar, M., Nepf, H., 2016. Wave-induced dynamics of flexible blades. J. Fluids Struct. 61, 20–41.

Manca, E., Cáceres, I., Alsina, J., Stratigaki, V., Townend, I., Amos, C., 2012. Wave energy and wave-induced flow reduction by full-scale model posidonia oceanica seagrass. Cont. Shelf Res. 50, 100–116.

Massel, S.R., 1983. Harmonic generation by waves propagating over a submerged step. Coast. Eng. 7, 357–380.

Maza, M., Lara, J.L., Losada, I.J., 2013. A coupled model of submerged vegetation under oscillatory flow using Navier–Stokes equations. Coast. Eng. 80, 16–34.

Mendez, F.J., Losada, I.J., 2004. An empirical model to estimate the propagation of random breaking and nonbreaking waves over vegetation fields. Coast. Eng. 51 (2), 103–118.

Méndez, F.J., Losada, I.J., Losada, M.A., 1999. Hydrodynamics induced by wind waves in a vegetation field. J. Geophys. Res.: Oceans 104 (C8), 18383–18396.

Morris, R.L., Konlechner, T.M., Ghisalberti, M., Swearer, S.E., 2018. From grey to green: Efficacy of eco-engineering solutions for nature-based coastal defence. Glob. Chang. Biol. 24 (5), 1827–1842.

Nepf, H.M., 2012. Flow and transport in regions with aquatic vegetation. Annu. Rev. Fluid Mech. 44, 123–142.

Olivé, I., Vergara, J., Pérez-Lloréns, J., 2013. Photosynthetic and morphological photoacclimation of the seagrass Cymodocea nodosa to season, depth and leaf position. Mar. Biol. 160, 285–297.

Ondiviela, B., Losada, I.J., Lara, J.L., Maza, M., Galván, C., Bouma, T.J., van Belzen, J., 2014. The role of seagrasses in coastal protection in a changing climate. Coast. Eng. 87, 158–168.

Paul, M., Amos, C., 2011. Spatial and seasonal variation in wave attenuation over Zostera noltii. J. Geophys. Res.: Oceans 116 (C8).

Pergent, G., Romero, J., Pergent-Martini, C., Mateo, M.-A., Boudouresque, C.-F., 1994. Primary production, stocks and fluxes in the Mediterranean seagrass Posidonia oceanica. Mar. Ecol. Prog. Ser. 139–146.

Sánchez-González, J.F., Sánchez-Rojas, V., Memos, C.D., 2011. Wave attenuation due to Posidonia oceanica meadows. J. Hydraul. Res. 49 (4), 503–514.

Schaffer, H., 1996. Second-order wavemaker theory for irregular waves. Ocean Eng. 23 (1), 47–88.

Soissons, L.M., Van Katwijk, M., Peralta, G., Brun, F., Cardoso, P., Grilo, T., Ondiviela, B., Recio, M., Valle, M., Garmendia, J., et al., 2018. Seasonal and latitudinal variation in seagrass mechanical traits across Europe: the influence of local nutrient status and morphometric plasticity. Limnol. Oceanogr. 63 (1), 37–46.

Stratigaki, V., Manca, E., Prinos, P., Losada, I.J., Lara, J.L., Sclavo, M., Amos, C.L., Cáceres, I., Sánchez-Arcilla, A., 2011. Large-scale experiments on wave propagation over Posidonia oceanica. J. Hydraul. Res. 49 (sup1), 31–43.

Sutton-Grier, A.E., Wowk, K., Bamford, H., 2015. Future of our coasts: The potential for natural and hybrid infrastructure to enhance the resilience of our coastal communities, economies and ecosystems. Environ. Sci. Policy 51, 137–148.

Taddei, S., Manes, C., Ganapathisubramani, B., 2016. Characterisation of drag and wake properties of canopy patches immersed in turbulent boundary layers. J. Fluid Mech. 798, 27–49.

Temmerman, S., Meire, P., Bouma, T.J., Herman, P.M., Ysebaert, T., De Vriend, H.J., 2013. Ecosystem-based coastal defence in the face of global change. Nature 504 (7478), 79–83.

Twomey, A.J., O'Brien, K.R., Callaghan, D.P., Saunders, M.I., 2020. Synthesising wave attenuation for seagrass: Drag coefficient as a unifying indicator. Mar. Pollut. Bull. 160, 111661.

Vettori, D., Marjoribanks, T., 2021. Temporal variability and within-plant heterogeneity in blade biomechanics regulate flow-seagrass interactions of Zostera marina. Water Resour. Res. 57 (3), e2020WR027747.

Vettori, D., Niewerth, S., Aberle, J., Rice, S., 2021. A link between plant stress and hydrodynamics? Indications from a freshwater macrophyte. Water Resour. Res. 57 (9), e2021WR029618.

Waycott, M., Duarte, C.M., Carruthers, T.J., Orth, R.J., Dennison, W.C., Olyarnik, S., Calladine, A., Fourqurean, J.W., Heck Jr., K.L., Hughes, A.R., et al., 2009. Accelerating loss of seagrasses across the globe threatens coastal ecosystems. Proc. Natl. Acad. Sci. 106 (30), 12377–12381.

Wooding, R., Bradley, E.F., Marshall, J., 1973. Drag due to regular arrays of roughness elements of varying geometry. Bound.-Lay. Meteorol. 5 (3), 285–308.